Research Letter **DOI:** 10.15541/jim20240433

Rare Earth Oxide Surface Modification of Porous SiO_2 Film Prepared by Atomic Layer Deposition

JIN Jianfei[1,2], LÜ Lin[1], LI Ying[1], YAN Lu[1], CAO Yunzhen[1], LI Wei[2]

(1. Key Laboratory of Inorganic Coating Materials CAS, Shanghai Institute of Ceramics, Chinese Academy of Sciences, Shanghai 200050, China; 2. School of Materials and Chemistry, University of Shanghai for Science and Technology, Shanghai 200093, China)

Abstract: Broadband transparent films play a pivotal role in various applications such as lenses and solar cells, particularly porous structured transparent films exhibit significant potential. This study investigates a porous SiO_2 refractive index gradient anti-reflective film prepared by atomic layer deposition (ALD). A porous SiO_2 film with gradual porosity was obtained by phosphoric acid etching of Al_2O_3/SiO_2 multilayers with gradient Al_2O_3 ratios, achieving a gradual decrease in refractive index from the substrate to the surface. The film exhibited an average transmittance as high as 97.8% within the wavelength range from 320 nm to 1200 nm. The environmental adaptability was further enhanced by surface modification using rare earth oxide (REO) La_2O_3, resulting in formation of a lotus leaf-like structure and achieving a water contact angle of 100.0°. These data proved that the modification significantly improved hydrophobic self-cleaning capability while maintaining exceptional transparency of the film. The surface structure of the modified film remained undamaged even after undergoing wipe testing, demonstrating its excellent surface durability.

Key words: porous SiO_2; rare earth oxide; atomic layer deposition; anti-reflective; self-cleaning

Broadband anti-reflective coatings exhibit remarkable transmittance across a wide spectrum ranging from visible to near-infrared wavelengths, finding extensive applications in contemporary optical systems[1-3]. The film design of this material now predominantly relies on a multilayer structure, with the typical fabrication methods mainly including physical vapor deposition (PVD)[4] and chemical vapor deposition (CVD) techniques, such as evaporation, sputtering, and plasma-enhanced CVD. By utilizing the interference cancellation effect of alternating films, typically high refractive index materials (like ZrO_2 or HfO_2) combined with low refractive index materials (like Al_2O_3 or MgF_2), an anti-reflection effect is achieved. In comparison, the reduction of reflection in gradient refractive index films is achieved through low refractive index as well as the elimination of interface between the film and substrate. MgF_2 possesses a refractive index of 1.38, which is the lowest among existing options. It is therefore desirable to fabricate film materials with refractive indices lower than that of MgF_2. Thin film with porous structure can greatly reduce its refractive index and have significant application in flat-panel displays[5], photovoltaics[6] and other optical systems, thus various porous films with refractive index lower than 1.38 have been fabricated, such as TiO_2[7] and SiO_2[8-10].

Recently, Ghazaryan *et al*.[11-13] proposed the use of ALD to prepare Al_2O_3/SiO_2 multilayers on a quartz substrate, which were subsequently etched with phosphoric acid to obtain a porous SiO_2 structure, but the film was fragile. The refractive index of the structure was reduced from 1.47 (the refractive index of the quartz substrate) to 1.13, and Rayleigh scattering can be neglected[14]. This porous SiO_2 film on quartz is equivalent to a monolayer anti-reflective coating, showing an elevated transmittance. Simultaneously, the porous structure altered the hydrophilicity and hydrophobicity properties[15-16]. One significant advantage of the ALD technique lies in its exceptional conformality and repeatability, which greatly facilitates the precise coating of multilayer anti-reflective films on curved surfaces such as cylinders or semicircular lenses[17].

Received date: 2024-10-14; **Revised date:** 2024-11-09; **Published online:** 2024-12-16
Biography: JIN Jianfei (1996–), male, Master candidate. E-mail: jinjianfei98@163.com
金剑飞(1996–), 男，硕士研究生. E-mail: jinjianfei98@163.com
Corresponding author: CAO Yunzhen, professor. E-mail: yzhcao@mail.sic.ac.cn; LI Wei, professor. E-mail: liwei176@usst.edu.cn
曹韫真，研究员. E-mail: yzhcao@mail.sic.ac.cn; 李 伟，教授. E-mail: liwei176@usst.edu.cn

The hydrophobic self-cleaning capability is another important performance feature of broadband anti-reflective materials used in foggy conditions, such as swimming goggles. Applying a hydrophobic silane coating on the surface is a commonly employed technique, however, its efficacy may diminish following wiping[18]. REOs are excellent surface modification materials. Azimi *et al*.[19-22] reported that the entire REOs are inherently hydrophobic and capable of withstanding high-temperature treatments and severe friction. This occurs because REOs are highly prone to adsorbing hydrocarbons in environments, which reduces their surface energy[23-27]. The Yb_2O_3 film prepared using ALD method exhibits a water contact angle of 95° for a thickness of 20 nm upon exposure to ambient air[28]. Similar results were documented using lanthanide REOs[25, 29]. In addition, a lotus leaf structure is a widely reported biomimetic hydrophobic architecture[30-34].

In this study, Al_2O_3/SiO_2 multilayers with gradient Al_2O_3 ratios were prepared using ALD, and a porous SiO_2 film possessing gradual porosity was successfully obtained after phosphoric acid etching. This film exhibited a refractive index gradation and showed a refined balance between its robustness and transparency, achieving an average transmittance of up to 97.8% across a wide wavelength band (320–1200 nm). To enhance the self-cleaning capability as well as the environmental adaptability of the film, a La_2O_3 film with lotus leaf structure was further deposited on the porous SiO_2 film using ALD. The water contact angle of the film increased from 5° to 100°, showing remarkable anti-fogging properties. Additionally, it showed significantly better environmental adaptability after wiping test in comparison to the monolayer SiO_2 film, indicating that this film is promising for application in precision optics under harsh environmental conditions.

1 Experimental

1.1 Materials and methods

SiO_2 glass of 99.99% purity was used as the substrate and was cleaned in the ultrasonic bath for 10 min prior to use. Al_2O_3/SiO_2 multilayers and La_2O_3 films were deposited using an ALD equipment (TFS 500, Beneq, Finland).

The precursors trimethylaluminium (TMA), diisopropylaminosilane (DIPAS) and La tris (*N*,*N*′-diisopropylformamidinato) lanthanum (La(^{i}PrfAMD)$_3$) were used for the deposition of Al_2O_3, SiO_2 and La_2O_3, respectively. The preparation conditions are shown in Table 1.

The growth rates of the Al_2O_3 and SiO_2 films were 0.1 and 0.085 nm per cycle, respectively. In this work, the number of cycles of each SiO_2 layer was fixed at 7 and the thickness was 0.6 nm, while the thickness of each Al_2O_3 layer was varied, with respective values of 0.6, 0.9, 1.2, and 1.5 nm. The Al_2O_3/SiO_2 multilayers were deposited at 350 ℃ from repeated ALD cycles with a gradient thickness ratio of 2/3/4/5 : 2 for Al_2O_3 to SiO_2, respectively, as illustrated in Fig. 1(a). After the ALD of Al_2O_3/SiO_2 multilayers, the Al_2O_3 layer could be selectively wet chemical etched in 85% H_3PO_4 solution at 25 ℃ for 24 h, and a nanoporous (NP) SiO_2 layer was obtained[16], exhibiting a graded porous structure, as shown in Fig. 1(b).

La_2O_3 film was deposited on the surface of NP SiO_2 films. In the La_2O_3 deposition process, plasma oxygen (O_2) was used for oxidizing the La-ligand[35], with a power of 60 W and a plasma time of 5 s, and the growth rate was 0.1 nm per cycle. The thickness of La_2O_3 film was fixed at 20 nm. Plasma oxygen utilization effectively suppresses the formation of La hydroxides, where O–La–O bonding dominates the deposition of La, ensuring compliance with the self-limiting nature of ALD[36].

1.2 Characterization

The microstructure of the anti-reflective (AR) system was investigated using a field emission scanning electron microscope (FE-SEM, Verios G4 UC, Thermo scientific, America). The refractive index was measured using an ellipsometer with an angle of 65° (V-VASE, J. A. Woollam, America). The reflectance and transmittance spectra were recorded using a UV-Vis-NIR spectrophotometry (UH4150, HITACH, Japan). The water contact angle test was performed using a fluorescence spectrum analysis test platform (Fluoromax4, HORIBA, Japan). The wipe resistance test was evaluated according to the ASTM F2357 RCA tape friction standard test methods using an RCA paper tape wear testing machine (ZJ-7-IBB, ZHIJAI, China). The load is 55 g. The experimental

Table 1 Preparation parameters of films

Material	First reactant (pulse time)	First purge (purge time)	Second reactant (pulse time)	Second purge (purge time)	Deposition temperature/℃
Al_2O_3	TMA (0.15 s)	N_2 (1.5 s)	H_2O (0.1 s)	N_2 (1.5 s)	350
SiO_2	DIPAS (0.10 s)	N_2 (1.5 s)	O_3 (1.0 s)	N_2 (1.5 s)	350
La_2O_3	La(^{i}PrfAMD)$_3$ (0.10 s)	N_2 (1.5 s)	Plasma-O_2 (5.0 s)	N_2 (1.5 s)	250

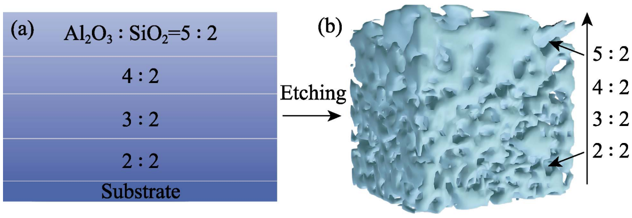

Fig. 1　Diagram of the film structure
(a) Schematic diagram of the Al_2O_3/SiO_2 multilayers with gradient Al_2O_3 ratios; (b) 3D structure of NP SiO_2 film with a gradient index

results quantified the number of standard rotations to evaluate the extent of film damage following an equal number of wiping cycles.

The porosity of the film is calculated by Equation (1):

$$P = \frac{N_1^2 - N_P^2}{N_1^2 - 1} \tag{1}$$

where P represents the porosity of porous film, N_1 represents the refractive index of glass, and N_P represents the refractive index of porous film[37].

The SiO_2 glass substrate, NP SiO_2 films without and with La_2O_3 modification were subjected to steam and frozen testing to evaluate their anti-fogging performance[16]. Specifically, the samples were placed above a petri dish containing boiling water. The condensation of steam on the glass surface was observed and photographed. Frozen testing was conducted by placing the samples in a refrigerator at –18 ℃ for 1 h and then placed in the humid laboratory air. The condensation of steam on the glass surface was observed and photographed. The samples were placed in a C-shaped pattern, and the transparency performance could be visually observed after tests.

2　Results and discussion

2.1　Morphology analysis of NP SiO_2 films

Fig. 2 shows the surface morphologies of NP SiO_2 films with different Al_2O_3/SiO_2 thickness ratios after phosphoric acid etching for 24 h. In Fig. 2(a), with a Al_2O_3/SiO_2 ratio of 2∶2, the film exhibits a pore size range of 6–8 nm in diameter. With the increasing Al_2O_3 ratio, the pore size increases gradually to 30 nm in diameter, which interconnects and forms a porous framework (Fig. 2(d)).

Fig. 3(a-c) show the cross-sectional FE-SEM images of NP SiO_2 films after different etching times, ranging from 3 h to 24 h. 85% H_3PO_4 reacts with the film surface, and etching proceeds gradually from top to bottom, transforming the film into a porous structure. After a 24 h-etching process, the Al_2O_3 is fully corroded, resulting in the formation of porous silicon dioxide.

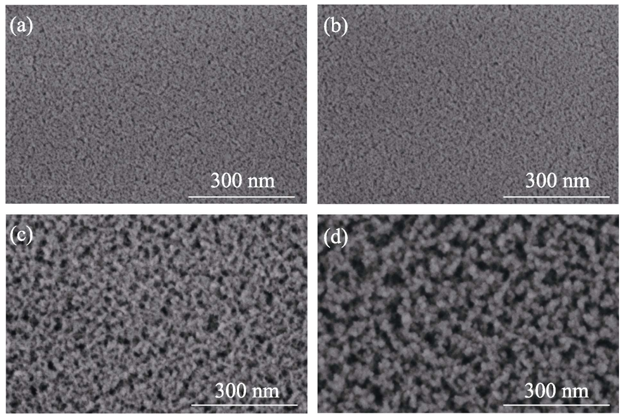

Fig. 2　SEM images after acid etching of Al_2O_3/SiO_2 multilayers with thickness ratios at (a) 2∶2, (b) 3∶2, (c) 4∶2, and (d) 5∶2

Therefore, a final etching duration of 24 h is selected. During the etching process, the entirety of the Al_2O_3 layer is eradicated, causing the collapse of SiO_2 layer and the rupture of Al–O–Si bonds. This rupture facilitates the formation of new Si–O–Si bonds, resulting in the reconfiguration into novel siloxane hydroxylation bonds, thus transitioning into a porous structure. Due to hydroxylation and intricate reassembly, nanopores interconnect, forming a porous network[11-12]. In the experiment, a SiO_2 layer is observed with a thickness exceeding 0.9 nm and acts as a barrier, impeding the reaction between H_3PO_4 and Al_2O_3 layers. Therefore, another possibility is proposed. As depicted in Fig. 3(d), when the silica layer is thin (*e.g.*, 0.6 nm in this experiment), a monolayer of silica does not completely cover the surface. In certain regions within the silica layer, a minor fraction of aluminum oxide atoms is interspersed, compromising the ability of the silica layer to fully impede contact with phosphoric acid. Consequently, phosphoric acid gradually reacts with the underlying aluminum oxide layer throughout the stack while leaving behind remnants of the silica layer.

In order to validate this perspective, the thickness of the SiO_2 layer in the Al_2O_3/SiO_2 films ranging from 0.3 nm to 1.5 nm was modified. The thickness of Al_2O_3 layer was fixed at 0.6 nm, and each Al_2O_3/SiO_2 thickness ratio film was deposited 10 times, followed by a 24-h acid etching process. Fig. 3(e) indicates that the Al_2O_3/SiO_2 films have a thickness of 195 nm, with an acid etching depth of 65 nm. In this instance, the SiO_2 layer measures approximately 0.9 nm in thickness. The result reveals that the etching process comes to a complete halt when the SiO_2 layer reaches a relatively substantial thickness (>0.9 nm). The ALD method yields compact films, as illustrated in Fig. 3(f). However, at reduced thicknesses, complete coverage of the entire surface is not achieved, resulting in some porosity on the film surface. With increasing

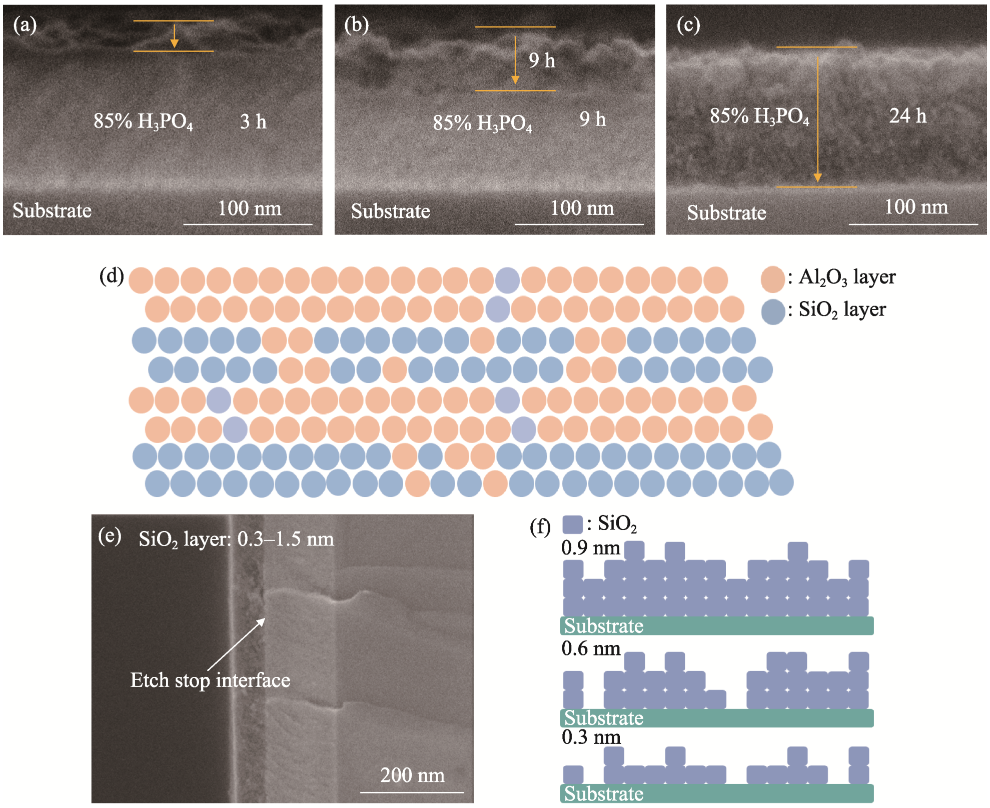

Fig. 3 FE-SEM images of cross sections and diagram of films

(a-c) Acid etching for (a) 3, (b) 9 and (c) 24 h; (d) Schematic diagram of acid etching conjecture Al_2O_3/SiO_2 layers; (e) Different thickness of SiO_2 layer in Al_2O_3/SiO_2 films after acid etching for 24 h; (f) Deposition diagram of SiO_2 layers with different thicknesses

Colorful figures are available on website

thickness, these small pores become effectively sealed.

2.2 Performance of NP SiO_2 films with graded refractive index

Fig. 4(a) shows the refractive index of NP SiO_2 films with different Al_2O_3/SiO_2 ratios after 85% H_3PO_4 etching for 24 h. At a ratio of 2∶2, the refractive index is 1.29, corresponding to a porosity of 40%, as calculated using Equation (1). As the Al_2O_3 content increases, the refractive index decreases. At a ratio of 5∶2, the refractive index decreases to 1.14, corresponding to a porosity of 75%. The gradient film has an average porosity of 56%. The results correlate with the morphologies in Fig. 2, where increasing Al_2O_3 content leads to larger SiO_2 framework, larger pore size, higher porosity, and a gradual decrease in refractive index. Fig. 4(b) shows the transmittance of NP SiO_2 films with different Al_2O_3/SiO_2 ratios after phosphoric acid etching for 24 h. It can be observed that the fixed refractive index of NP SiO_2 films exhibits a single peak in transmittance, which is relatively narrow. In contrast, the NP SiO_2 films with gradient refractive index exhibit high transmittance across a broad wavelength range of 320–1200 nm, showcasing excellent wideband optical transparency.

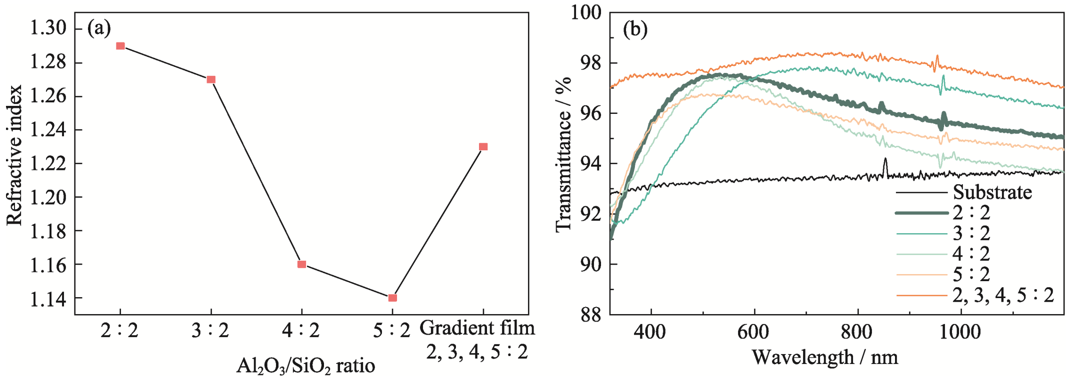

Fig. 4 Performance of NP SiO_2 films with different Al_2O_3/SiO_2 thickness ratios

(a) Refractive index at 580 nm; (b) Transmittance curves. Colorful figures are available on website

Fig. 5 shows the water contact angle (WCA) test result of NP SiO_2 films with gradient refractive index, where the water droplet spreads almost completely on surface, maintaining a low WCA of less than 5° (4.5°±0.5°). The results indicate that this film exhibits excellent hydrophilicity, which can be attributed to its porous framework and the inherent hydrophilic nature of SiO_2[15-16, 38].

2.3 Morphology and performance of La_2O_3-modified NP SiO_2 films

Multifunctionality is also critical for practical engineering applications such as energy harvesting and operation of optical instruments in extreme climates or humid conditions[30]. In order to improve the film's self-cleaning capability and environmental adaptability, the deposition of REOs on the surface of NP SiO_2 films is proposed (Fig. S1)[39-41]. Fig. 6(a) shows a cross-sectional view of the film at a 45° inclination, with a 20 nm La_2O_3 layer on top and a graded refractive index NP SiO_2 film layer below.

Fig. 6(b) presents the transmittance of surface-modified films. The transmittance curve of La_2O_3-modified NP SiO_2 films does not exhibit a discernible peak across the entire wavelength range, resembling the observed trend of NP SiO_2 films. The transmittance in the range of 600–1000 nm exhibits a slight reduction compared to the NP SiO_2 films, but still remains as high as 95%. This result indicates that the films still possess wideband antireflection property after La_2O_3 modification.

Fig. 7(a, b) depict the planar morphology and WCA test results of the La_2O_3 film deposited directly on SiO_2 glass. The La_2O_3 film exhibits a film morphology with a few particle aggregations, with sizes ranging from 20 nm to 30 nm. The WCA is measured to be 83.0°±0.5°. In Figs. 7(c, d), La_2O_3 is deposited on the NP SiO_2 films, resulting in a particulate growth and agglomerated film, leading to a WAC of 100.0°±0.5°, thus bestowing hydrophobicity upon the film. The transformation of the film into a lotus leaf-like structure leads to an increase in surface roughness. This unique surface structure traps a thin layer of air, resulting in a significant reduction in the contact area between water droplets and the rough surface. As a result, water infiltration into the surface structure is effectively prevented[30-34, 42]. Moreover, the REOs films absorb hydrocarbons in the air, lowering the surface energy and transforming the film from hydrophilic to hydrophobic[43]. Compared to the result shown in Fig. 5, the WCA increased significantly from less than 5° to 100°, thereby greatly enhancing the hydrophobic performance of the modified film. Additionally, the presence of a dense surface structure effectively prevents airborne small particles from contaminating the porous SiO_2 film. The hydrophobic properties of the film are maintained even after 6 months of exposure to ambient air.

Due to the inherent chemical characteristics of ALD process, the substrate surface plays a pivotal role in ALD fabrication. In cases where the initial growth surface is not conducive to the reaction of the La precursor, growth can only occur at specific sites, leading to a Volmer-Weber island growth mode and resulting in the aggregation of La_2O_3[44-46].

Fig. 7(e, f) show the fogging test results, including freeze and steam tests. Under freezing conditions, the SiO_2 glass quickly fogged up, while the modified film maintained a higher level of clarity. In steam test, the SiO_2 glass becomes visibly foggy, resulting in decreased transparency, while the modified film forms droplets of water, resulting in excellent transparency. The results

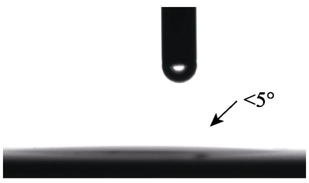

Fig. 5　WCA test result of NP SiO_2 films

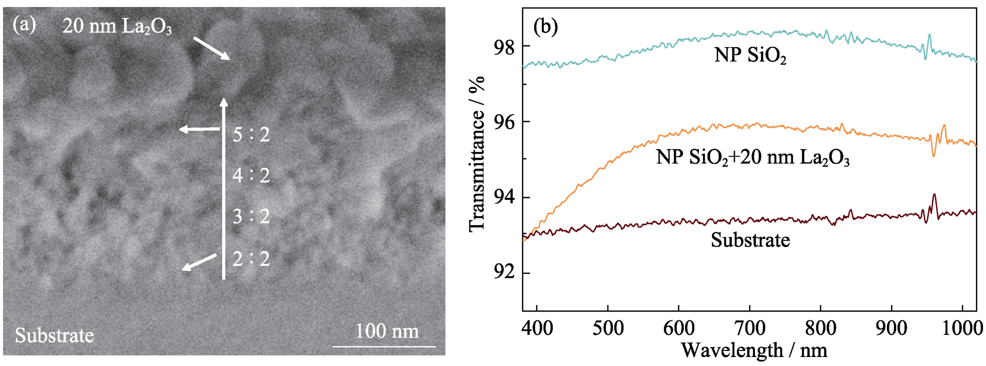

Fig. 6　Morphology and performance of the film

(a) 45° cross-section morphology of NP SiO_2 films with La_2O_3 modification; (b) Transmittance curves of different samples

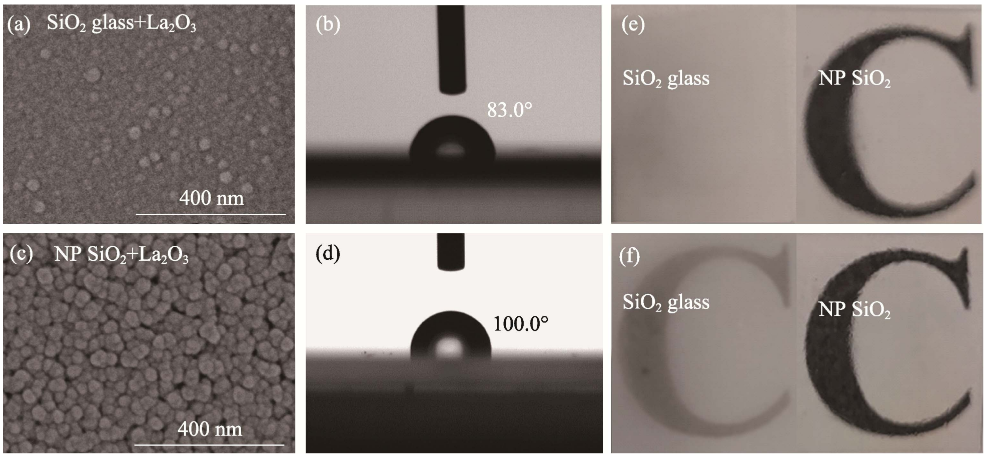

Fig. 7 SEM images and WCA test results

(a, b) La_2O_3 film on SiO_2 glass; (c, d) La_2O_3 film on NP SiO_2 films; (e, f) Fogging results of (e) freeze test and (f) steam test

indicate that the modified film exhibits exceptional anti-fogging performance in freezing and steam tests while maintaining excellent transparency.

Fig. 8 illustrates the wipe test results of the samples. As shown in Fig. 8(a), the NP SiO_2 films without La_2O_3 modification show a loose structure, leading to noticeable tearing after 50 cycles of friction[47]. In comparison, after an equal number of friction cycles, no discernible traces of tearing are observed on the La_2O_3-modified NP SiO_2 films (Fig. 8(b)), indicating a significant improvement in wipe resistance. The compact structure of La_2O_3 films prepared by the ALD method enhances their structural integrity. Moreover, the spherical morphology of La_2O_3 particles might also reduce resistance during surface wiping.

It is worth noting that in most hydrophobic coating methods, such as applying a hydrophobic organic compound onto a film, the surface compound is highly susceptible to frictional wear, leading to a gradual decrease in surface hydrophobicity over time or after wiping[18, 48]. However, REOs modified films exhibit remarkable durability by maintaining a certain degree of hydrophobicity even after being wiped due to their exceptional ability to adsorb hydrocarbons from the surrounding air and thereby reduce surface energy (Fig. 8(c)). Consequently, these films can effectively restore their hydrophobic properties through continuous absorption of hydrocarbons even after experiencing surface abrasion[24, 27].

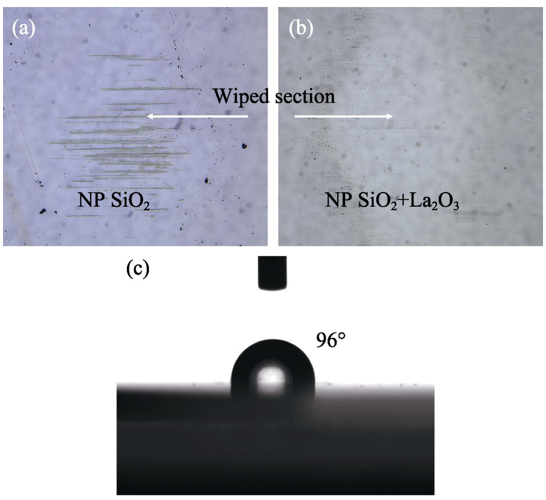

Fig. 8 Results of the wipe resistance test

(a) NP SiO_2 films; (b) La_2O_3-modified NP SiO_2 films; (c) WCA test result of La_2O_3-modified NP SiO_2 films after being wiped

3 Conclusions

In this study, NP SiO_2 films with gradient refractive index are proposed, along with their surface modification using REOs by ALD. The refractive index gradient is achieved on a single-layer film by varying the Al_2O_3/SiO_2 ratio and post-etching, resulting in significant anti-reflection effects in a wide wavelength range of 320–1200 nm. After REOs modification, La_2O_3 particles are densely packed, forming a lotus leaf-like structure, and by absorbing hydrocarbons from the air, the La_2O_3-modified films achieve a WCA of 100°, significantly enhancing the self-cleaning capability. Additionally, the La_2O_3-modified NP SiO_2 films exhibit excellent wipe resistance and environmental adaptability.

Supporting materials

Supporting materials related to this article can be found at https://doi.org/10.15541/jim20240433.

References:

[1] RAY N J, YOO J H, NGUYEN H T, *et al*. All-glass metasurfaces for ultra-broadband and large acceptance angle antireflectivity: from ultraviolet to mid-infrared. *Advanced Optical Materials*, 2023,

11(12): 2300137.

[2] WU J, TU J, LI L, *et al*. Gradient refractive index-based broadband antireflective coatings and application in silicon solar modules. *Surfaces and Interfaces*, 2022, **30:** 101918.

[3] SUN X, HU K, TU J, *et al*. Design and preparation of superhydrophobic, broadband and double-layer antireflective coatings. *Surfaces and Interfaces*, 2021, **24:** 101135.

[4] RUUD C J, CLERI A, MARIA J P, *et al*. Ultralow index SiO_2 antireflection coatings produced *via* magnetron sputtering. *Nano Letters*, 2022, **22(18):** 7358.

[5] LI Y, ZHANG J, ZHU S, *et al*. Biomimetic surfaces for high-performance optics. *Advanced Materials*, 2009, **21(46):** 4731.

[6] DONG S, ZHANG J, JIAO H, *et al*. Nanopillars assisted multilayer antireflection coating for photovoltaics with multiple bandgaps. *Applied Physics Letters*, 2019, **115(13):** 133106.

[7] KIM S H, LEE S H, YU J S. Broadband and antireflective characteristics of glancing angle deposited titanium dioxide nanostructures for photovoltaic applications. *Thin Solid Films*, 2019, **685:** 53.

[8] XI J Q, KIM J K, SCHUBERT E F. Silica nanorod-array films with very low refractive indices. *Nano Letters*, 2005, **5(7):** 1385.

[9] TAO C, ZOU X, REDDY K M, *et al*. A hydrophobic ultralow refractive-index silica coating towards double-layer broadband antireflective coating with exceptionally high vacuum stability and laser-induced damage threshold. *Colloids and Surfaces A: Physicochemical and Engineering Aspects*, 2019, **563:** 340.

[10] YE L, LI L, WANG X, *et al*. Template-free synthesis of uniform hollow silica nanoparticles for controllable antireflection coatings. *Ceramics International*, 2020, **46(6):** 7453.

[11] GHAZARYAN L, KLEY E B, TUNNERMANN A, *et al*. Nanoporous SiO_2 thin films made by atomic layer deposition and atomic etching. *Nanotechnology*, 2016, **27(25):** 255603.

[12] GHAZARYAN L, SEKMAN Y, SCHRÖDER S, *et al*. On the properties of nanoporous SiO_2 films for single layer antireflection coating. *Advanced Engineering Materials*, 2019, **21(6):** 1801229.

[13] GHAZARYAN L, KLEY E B, TÜNNERMANN A, *et al*. Composite materials and nanoporous thin layers made by atomic layer deposition. *Optical Systems Design 2015: Advances in Optical Thin Films V*, 2015, **9627:** 96270P.

[14] SEKMAN Y, FELDE N, GHAZARYAN L, *et al*. Light scattering characterization of single-layer nanoporous SiO_2 antireflection coating in visible light. *Applied Optics*, 2020, **59(5):** A143.

[15] CEBECI F Ç, WU Z Z, ZHAI L. Nanoporosity-driven superhydrophilicity: a means to create multifunctional antifogging coatings. *Langmuir*, 2006, **22:** 2856.

[16] CHEN J, ZHANG L, ZENG Z, *et al*. Facile fabrication of antifogging, antireflective, and self-cleaning transparent silica thin coatings. *Colloids and Surfaces A: Physicochemical and Engineering Aspects*, 2016, **509:** 149.

[17] PFEIFFER K, GHAZARYAN L, SCHULZ U, *et al*. Wide-angle broadband antireflection coatings prepared by atomic layer deposition. *ACS Applied Materials & Interfaces*, 2019, **11(24):** 21887.

[18] WANG X, ZHAO H, CAO Y, *et al*. Surface free energy and microstructure dependent environmental stability of Sol-Gel SiO_2 antireflective coatings: effect of combined vapor phase surface treatment. *Journal of Colloid and Interface Science*, 2019, **555:** 124.

[19] AZIMI G, DHIMAN R, KWON H M, *et al*. Hydrophobicity of rare-earth oxide ceramics. *Nature Materials*, 2013, **12(4):** 315.

[20] KUJAWA J, AL-GHARABLI S, WRZESZCZ G, *et al*. Physicochemical and magnetic properties of functionalized lanthanide oxides with enhanced hydrophobicity. *Applied Surface Science*, 2021, **542:** 148563.

[21] TAN X, ZHU D, SHI Z, *et al*. Thickness-dependent morphology, microstructure, adsorption and surface free energy of sputtered CeO_2 films. *Ceramics International*, 2020, **46(9):** 13925.

[22] LV Q, ZHANG S, DENG S, *et al*. Transparent and water repellent ceria film grown by atomic layer deposition. *Surface and Coatings Technology*, 2017, **320:** 190.

[23] KULAH E, MAROT L, STEINER R, *et al*. Surface chemistry of rare-earth oxide surfaces at ambient conditions: reactions with water and hydrocarbons. *Scientific Reports*, 2017, **7:** 43369.

[24] OH J, OREJON D, PARK W, *et al*. The apparent surface free energy of rare earth oxides is governed by hydrocarbon adsorption. *iScience*, 2022, **25(1):** 103691.

[25] OH I K, ZENG L, KIM J E, *et al*. Surface energy change of atomic-scale metal oxide thin films by phase transformation. *ACS Nano*, 2020, **14(1):** 676.

[26] FU S P, ROSSERO J, CHEN C, *et al*. On the wetting behavior of ceria thin films grown by pulsed laser deposition. *Applied Physics Letters*, 2017, **110(8):** 081601.

[27] XU P, MENG G, PERSHIN L, *et al*. Control of the hydrophobicity of rare earth oxide coatings deposited by solution precursor plasma spray by hydrocarbon adsorption. *Journal of Materials Science & Technology*, 2021, **62:** 107.

[28] ZHAO B, MATTELAER F, RAMPELBERG G, *et al*. Thermal and plasma-enhanced atomic layer deposition of yttrium oxide films and the properties of water wettability. *ACS Applied Materials & Interfaces*, 2020, **12(2):** 3179.

[29] OH I K, KIM K, LEE Z, *et al*. Hydrophobicity of rare earth oxides grown by atomic layer deposition. *Chemistry of Materials*, 2014, **27(1):** 148.

[30] PARK K C, CHOI H, CHANG C H, *et al*. Nanotextured silica surfaces with robust superhydrophobicity and omnidirectional broadband supertransmissivity. *ACS Nano*, 2012, **6:** 3789.

[31] SON J, KUNDU S, VERMA L K, *et al*. A practical superhydrophilic self cleaning and antireflective surface for outdoor photovoltaic applications. *Solar Energy Materials and Solar Cells*, 2012, **98:** 46.

[32] WANG D, WANG Z, ZHANG Z, *et al*. Both antireflection and superhydrophobicity structures achieved by direct laser interference nanomanufacturing. *Journal of Applied Physics*, 2014, **115(23):** 233101.

[33] HUANG Z, CAI C, KUAI L, *et al*. Leaf-structure patterning for antireflective and self-cleaning surfaces on Si-based solar cells. *Solar Energy*, 2018, **159:** 733.

[34] HAN G, NGUYEN T B, PARK S, *et al*. Moth-eye mimicking solid slippery glass surface with icephobicity, transparency, and self-healing. *ACS Nano*, 2020, **14(8):** 10198.

[35] KIM J Y, KIM H C, WALLACE R M, *et al*. *In situ* XPS study on ALD (atomic layer deposition) of high-*k* dielectrics La_2O_3 using La-formidinate and ozone. *ECS Transactions*, 2012, **45(3):** 95.

[36] LEE B, PARK T J, HANDE A, *et al*. Electrical properties of atomic-layer-deposited La_2O_3 films using a novel La formamidinate precursor and ozone. *Microelectronic Engineering*, 2009, **86(7/8/9):** 1658.

[37] YANG Z Y, ZHU D Q, LU D S, *et al*. The relationship between porous ratio and refractive index in nanoporous film. *Acta Optica Sinica*, 2003, **23(1366):** 1366.

[38] ESHAGHI A, MOJAB M. Fabrication of antireflective antifogging nano-porous silica thin film on glass substrate by layer-by-layer assembly method. *Journal of Non-Crystalline Solids*, 2014, **405:** 148.

[39] TAM J, PALUMBO G, ERB U, *et al*. Robust hydrophobic rare earth oxide composite electrodeposits. *Advanced Materials Interfaces*, 2017, **4(24):** 1700850.

[40] LUNDY R, BYRNE C, BOGAN J, *et al*. Exploring the role of

adsorption and surface state on the hydrophobicity of rare earth oxides. *ACS Applied Materials & Interfaces*, 2017, **9(15):** 13751.

[41] OH S, SHIM J, SEO D, *et al*. Organic/inorganic hybrid cerium oxide-based superhydrophobic surface with enhanced weather resistance and self-recovery. *Progress in Organic Coatings*, 2022, **170:** 106998.

[42] XU P, COYLE T W, PERSHIN L, *et al*. Understanding the correlations between the mechanical robustness, coating structures and surface composition for highly-/super-hydrophobic ceramic coatings. *Surface and Coatings Technology*, 2019, **378:** 124929.

[43] PRAKASH S, GHOSH S, PATRA A, *et al*. Intrinsic hydrophilic nature of epitaxial thin-film of rare-earth oxide grown by pulsed laser deposition. *Nanoscale*, 2018, **10(7):** 3356.

[44] CHEN P Y, HADAMEK T, KWON S, *et al*. Role of template layers for heteroepitaxial growth of lanthanum oxide on GaN(0001) *via* atomic layer deposition. *Journal of Vacuum Science & Technology A*, 2020, **38(1):** 012403.

[45] PUURUNEN R L, VANDERVORST W. Island growth as a growth mode in atomic layer deposition: a phenomenological model. *Journal of Applied Physics*, 2004, **96(12):** 7686.

[46] GEORGE S M. Atomic layer deposition: an overview. *Chemical Reviews*, 2010, **110(1):** 111.

[47] AYTUG T, LUPINI A R, JELLISON G E, *et al*. Monolithic graded-refractive-index glass-based antireflective coatings: broadband/omnidirectional light harvesting and self-cleaning characteristics. *Journal of Materials Chemistry C*, 2015, **3(21):** 5440.

[48] ZHANG C, KALULU M, SUN S, *et al*. Environmentally safe, durable and transparent superhydrophobic coating prepared by one-step spraying. *Colloids and Surfaces A: Physicochemical and Engineering Aspects*, 2019, **570:** 147.

原子层沉积法制备稀土氧化物表面改性多孔 SiO_2 薄膜

金剑飞[1,2], 吕 林[1], 李 莹[1], 闫 璐[1], 曹韫真[1], 李 伟[2]

(1. 中国科学院 上海硅酸盐研究所, 特种无机涂层重点实验室, 上海 200050; 2. 上海理工大学 材料与化学学院, 上海 200093)

摘 要: 宽带增透膜在透镜和太阳能电池等领域具有广泛应用, 其中多孔结构增透膜表现出巨大潜力。本工作研究了一种由原子层沉积(ALD)法制备的多孔 SiO_2 折射率梯度减反射膜。通过磷酸刻蚀 Al_2O_3/SiO_2 多层膜, 得到具有渐变孔隙率的多孔 SiO_2 膜, 折射率从衬底到表面逐渐降低。在 320~1200 nm 波长范围内, 薄膜的平均透过率达 97.8%。利用稀土氧化物 La_2O_3 表面改性, 薄膜表面形成荷叶状疏水结构, 水接触角为 100.0°, 在保持薄膜透过率的同时显著提高了疏水自清洁能力。改性薄膜在擦拭测试后未受到破坏, 表明其具有优异的表面耐久性, 而且环境适应性得到明显增强。

关 键 词: 多孔 SiO_2; 稀土氧化物; 原子层沉积; 减反射; 自清洁

中图分类号: TB43 **文献标志码:** A **文章编号:** 1000-324X(2025)09-1029-08

Supporting materials:

Rare Earth Oxide Surface Modification of Porous SiO_2 Film Prepared by Atomic Layer Deposition

JIN Jianfei[1,2], LÜ Lin[1], LI Ying[1], YAN Lu[1], CAO Yunzhen[1], LI Wei[2]

(1. Key Laboratory of Inorganic Coating Materials CAS, Shanghai Institute of Ceramics, Chinese Academy of Sciences, Shanghai 200050, China; 2. School of Materials and Chemistry, University of Shanghai for Science and Technology, Shanghai 200093, China)

The charge correction has been conducted utilizing the C element (284.8 eV). Fig. S1(a) showed wide-scan spectrum of the La_2O_3 layer. La and O elements were detected. In order to clarify the La valence state, peak fittings were performed as shown in Fig. S1(b). Regarding the La3d core level spectra, a splitting of the $La^{3+}3d_{5/2}$ and the $La^{3+}3d_{3/2}$ was observed. It has been reported the same split patterned peaks for the La3d emission profile, which can be attributed to configuration effects in the final state of La[1-2].

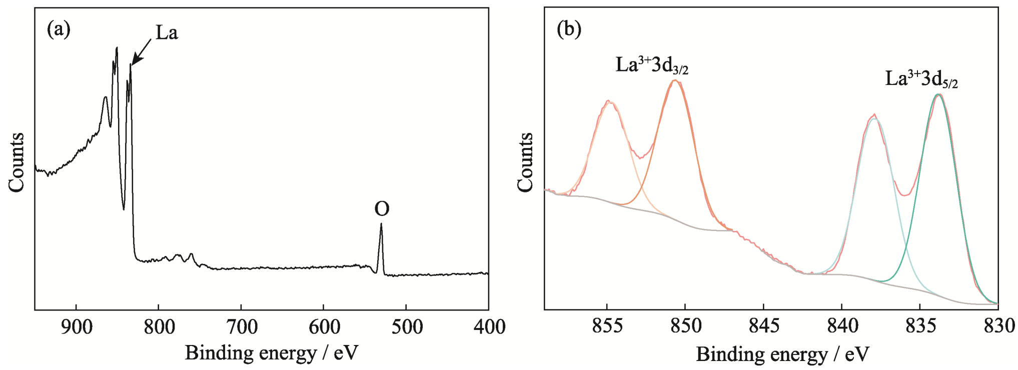

Fig. S1　XPS spectra of La_2O_3 layer

(a) Wide-scan spectrum; (b) $La^{3+}3d$ spectrum

References:

[1] AMAYA Á A, GONZÁLEZ C A, NIÑO-GÓMEZ M E, *et al*. XPS fitting model proposed to the study of Ni and La in deactivated FCC catalysts. *Journal of Electron Spectroscopy and Related Phenomena*, 2019, **233:** 5.

[2] RUIZ A M, CORNET A, MORANTE J R. Performances of La-TiO_2 nanoparticles as gas sensing material. *Sensors and Actuators B: Chemical*, 2005, **111/112:** 7.